Reprinted from APPLIED OPTICS, Vol. 8, page 893, May 1969

Features of Tropospheric and Stratospheric Dust

L. Elterman, R. Wexler, and D. T. Chang

A series of 119 profiles obtained over New Mexico comprise aerosol attenuation coefficients vs altitude to about 35 km. These profiles show the existence of several features. A surface convective dust layer extending up to about 5 km is seasonally dependent. Also, a turbidity maximum exists below the tropopause. The altitude of an aerosol maximum in the lower stratosphere is located just below that of the minimum temperature. The colder the minimum temperature, the greater is the aerosol content of the layer. This relationship suggests that the 20-km dust layer is due to convection in tropical air and advection to higher latitudes. Computed averages of optical thickness show that abatement of stratospheric dust from the Mt. Agung eruption became evident in April 1964. Results based on seventy-nine profiles characterizing volcanic dust abatement indicate that above 26 km, the aerosol scale height averages 3.75 km. Extrapolating with this scale height, tabulations are developed for uv, visible, and ir attenuation to 50 km. Optical mixing ratios are used to examine the aerosol concentrations at various altitudes, including a layer at 26 km having an optical thickness 10^{-3} for 0.55-μ wavelength.

I. Introduction

The aerosol content plays a significant role in the atmosphere's optical properties or, more quantitatively stated, the aerosol attenuation coefficient functions as an important optical parameter. As a first approximation, it is proportional to the aerosol number density. For a fixed wavelength, the height profile of this parameter, designated as $\beta_p(h,\lambda_1)$ provides information concerning aerosol concentration, presence of layers as well as optical thickness, which is necessary for determining atmospheric transmission for nonhorizontal path geometries. The aerosol attenuation coefficient and its profile have other important uses in studies entailing meteorological tracing, path radiance, sky background, possibly turbulence, and so on. Thus, the coefficient takes on the function of a fundamental parameter. Its measurement, however, has been difficult for a number of reasons. More basic than instrumentation difficulties are such factors as the atmosphere's variability, acquisition of *in situ* measurements to high altitudes, and results in the form of absolute values.

Acquiring information concerning a profile such as $\beta_p(h,\lambda_1)$ can best be done with optical methods, and a variety of these have been developed. Those which yielded absolute values are most suitable for comparing results and this is done in Fig. 1. The results were made comparable for $\lambda_1 = 0.55\ \mu$ by using the empirical relationship that the aerosol attenuation coefficient varies inversely with the wavelength. In order to represent the various methods of measurement as well as maintain clarity, not all results could be included in Fig. 1; i.e., the twilight measurements by Volz and Goody (1962) and by Rozenberg (1965), the searchlight measurements by Spankuch (1967), analysis of twilight aureole photographs from the spacecraft Vostok–6 (Driving, 1966), the aircraft measurements of sky brightness (Sandomirski *et al.* 1964), and aircraft nephelometry (Waldram, 1945). Also, interesting results in the form of relative values relating to β_p have been obtained with optical techniques: the twilight measurements (Bigg, 1964), laser beam backscatter (Collis and Ligda, 1966), (Clemeshaw *et al.* 1967), (Grams and Fiocco, 1967), and others. A consideration of all results indicates that the aerosol attenuation coefficient can be a widely varying parameter and that an adequate number of measurements are necessary in order to establish characteristic aerosol features.

For the purpose stated, recent searchlight probing measurements (Elterman, 1966a) are of interest for several reasons. First, a total of 119 profiles, $\beta_p(h,\lambda_1)$, were acquired and this represents a substantially larger sample than previously published. Additionally, each profile was obtained by measuring continuously through the troposphere and stratosphere with an altitude resolution approximating 1 km. Finally, we note in Fig. 1, that the mean of the profiles falls within the values determined by other researchers, a circumstance which affords a measure of comfort. An altas of the acquired profiles was presented previously (Elterman, 1966b). Now the objective is to consider the series of profiles statistically and in other ways in order

The first named author is with AFCRL, Bedford, Massachusetts 01730; the other authors are with Allied Research Associates, Inc., Concord, Massachusetts.

Received 16 December 1968.

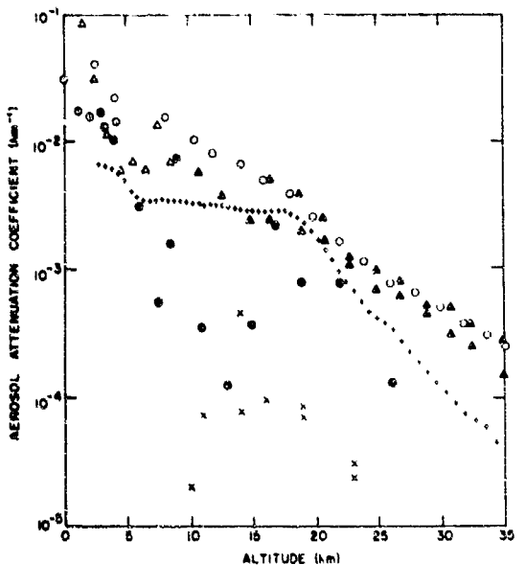

Fig. 1. Aerosol attenuation coefficients vs altitude at $\lambda_1 = 0.55\ \mu$. Comparison of results: ×, solar aureole, two balloon flights, Newkirk and Eddy (1964); △, solar radiation measured from aircraft, mean of eight flights, Penndorf (1954); +, searchlight probing, mean of 105 profiles, Elterman (1966a) and (1966b); ⊙, balloon integrating nephelometer, mean of fourteen flights, Crosby and Koerber (1962); ●, solar radiation measured from balloons, mean of three flights, Kondratiev *et al.* (1967); ▲, spacecraft horizon photography, analysis of four frames, Rozenberg (1966), Feoktistov (1965); ○, searchlight probing, mean for five nights, Rozenberg (1960, 1966).

to examine some tropospheric and stratospheric features.

II. Aerosol and Turbidity Profiles

Averaging a large number of profiles tends to wash out features readily noticed in the individual profile. We present therefore, in Fig. 2, an example of an individual profile chosen because (1) it is similar to the 119 profile average and (2) the aerosol features are sufficiently prominent.

The features of a profile can be examined also in terms of mixing ratios such that

$$\frac{\beta_p(h,\lambda)}{\beta_r(h,\lambda)} = \frac{\sigma_p(\lambda)}{\sigma_r(\lambda)} \frac{N_p(h)}{N_r(h)}, \tag{1}$$

where β_p and β_r are the aerosol and Rayleigh attenuation coefficients, respectively (cm^{-1}), N_p and N_r are the aerosol and molecular number densities, respectively (cm^{-3}). The terms σ_p and σ_r are the aerosol and molecular (Rayleigh) cross sections (cm^2). If up to 50 km the cross sections, both molecular and aerosol, tend to remain unchanged with altitude (a usual assumption), then Eq. (1) asserts that the optical mixing ratio β_p/β_r is proportional to the true mixing ratio, N_p/N_r. More frequently, the optical mixing ratio is known as turbidity. The turbidity profile corresponding to Fig. 2 is shown in Fig. 3. Here the 19-km dust region is evident as a prominent layer, partially due to increased aerosol content, but also because in this altitude region the $\beta_r(h,\lambda)$ values are diminished. For these reasons the turbidity profile has the advantage of improved aerosol feature emergence especially at the higher altitudes. However, when used in a qualitative sense only, assessment of the magnitude of the aerosol features can be difficult.

Since the volcanic dust in the atmosphere can have a residence time of several years, the effects of the Mt. Agung eruption (March 1963) must be considered. The direct measurements of Junge *et al.* (1961), Friend (1965), Mossop (1964), and Rosen (1968), collectively considered, before and after this event, show evidence of change in the stratospheric aerosol content. The observations of the twilight sky by Volz (1965), Meinel and Meinel (1964), and the analysis by Dyer and Hicks (1965) also show augmentation of stratospheric particulates. The searchlight probing measurements yielded absolute values of aerosol attenuation coefficients so that the most suitable parameter to use for examining this feature quantitatively is the stratospheric aerosol optical thickness for the stratospheric region to 25 km. The reason for choosing this altitude limit is discussed later. Accordingly, all profiles were placed in time sequential groups determined by the similarity of the stratospheric dust feature. Then the mean optical thickness was computed by

$$\bar{\tau} = \frac{1}{n} \sum_{i=1}^{n} \sum_{h_1}^{h_2} \bar{\beta}(h,\lambda_1)\Delta h, \tag{2}$$

where n is the number of profiles in the group, h_1 is the altitude of the tropopause, h_2 the 25-km altitude, $\bar{\beta}$ the mean aerosol attenuation coefficient (within each profile) for the altitude interval, and Δh the altitude

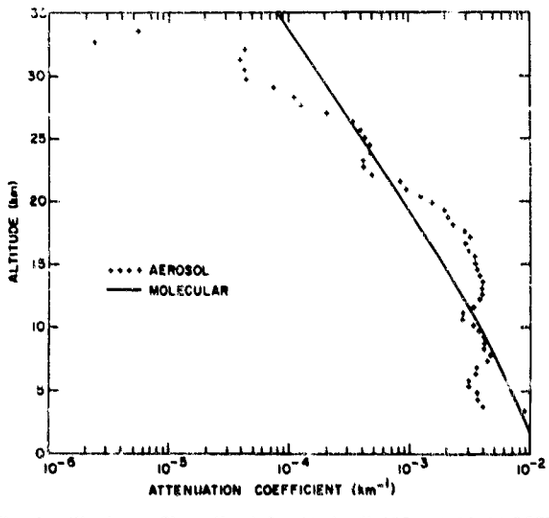

Fig. 2. Single profile $\beta_p(h,\lambda_1)$ for 11 April 1964 at 02:00 MST, similar to mean of 119 profiles, $\lambda_1 = 0.55\ \mu$. Surface to 5 km—convective region; 5–11.7 km—troposphere dust layer; 11.7–23.8 km—stratosphere dust layer; 25.6 km—upper altitude maximum; +, aerosol (measurements); — molecular (computed).

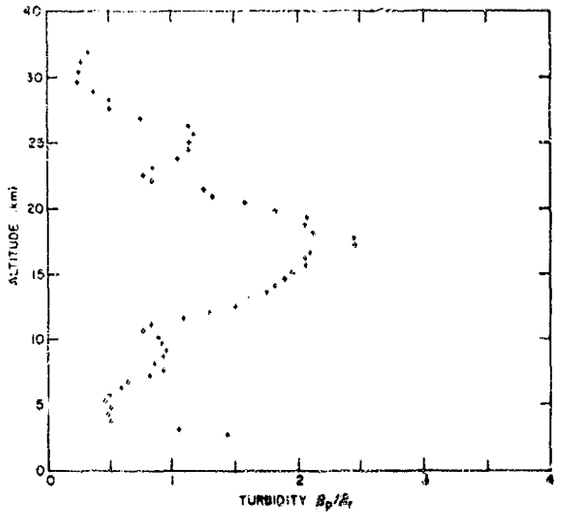

Fig. 3. Single turbidity profile $\beta_p(h,\lambda_1)/\beta_r(h,\lambda_1)$ for 11 April at 0200 MST. +, measurements (see caption for Fig. 2).

Table I. Aerosol Optical Thickness as a Measure of Volcanic Dust $\lambda_1 = 0.55\ \mu$

Group	Period (inclusive)	Number of profiles	Mean optical thickness (approximately 12–25 km) $\times 10^{-3}$
A	Dec. 1963–Mar. 1964	40	3.1
B	Apr. 1964–Sep. 1964	50	2.2
C	Oct. 1964–Nov. 1964	10	2.7
D	Dec. 1964–Apr. 1965	19	2.4
(B+C+D)	Apr. 1964–Apr. 1965	79	2.3

intervals used for computing the profiles. The results of this computation are presented in Table I.

Although the volcanic eruption occurred in March 1963, the tabulation shows that the volcanic dust component persisted over New Mexico up to and during the period December 1963 to March 1964. Beginning with April 1964, volcanic dust abatement and a generally stabilized level are indicated. The mean optical thickness computed for group (B + C + D) is 26% less than that of group A.

Parameters entailing the presence of volcanic dust may be unsuited for determining representative aerosol conditions. Accordingly, only the seventy-nine profiles characterized by volcanic dust abatement (group B + C + D of Table I) are used where required. In the discussion to follow, it is convenient to designate the seventy-nine profile mean for $\lambda_1 = 0.55\ \mu$ as $\bar{\beta}_p(h,\lambda_1)$. This and the corresponding turbidity profile are presented in Figs. 4 and 5.

The mean profile $\bar{\beta}_p(h,\lambda_1)$ in Fig. 4 can be extended to encompass a larger altitude range by using the aerosol scale height (H_p) relationship,

$$\bar{\beta}_p(h_2,\lambda_1) = \bar{\beta}_p(h_1,\lambda_1)\exp[-(h_2 - h_1)/H_p]. \quad (3)$$

This is a useful procedure because it facilitates development of atmospheric attenuation models (Sec. III) useful in exploratory calculation for the important 0–50-km altitude region. Penndorf's study (1954) shows that for the lowest 5 km, the aerosol coefficients fall off exponentially with a scale height $0.97 < H_p < 1.4$ km. We resort to the use of his mean value $H_p = 1.2$ km to extend the $\bar{\beta}_p(h,\lambda_1)$ profile from 3.7 km to

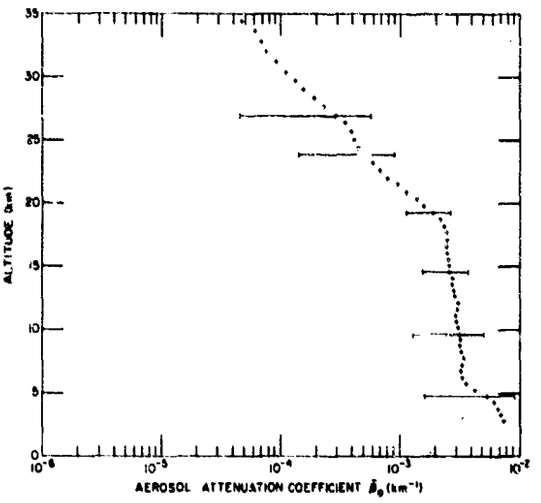

Fig. 4. Mean of seventy-nine low stratospheric dust profiles (Table I) for April 1964 to April 1965. Aerosol attenuation coefficients, $\bar{\beta}_p(h,\lambda_1)$; standard deviation limits attributable to error and atmospheric variations; $\lambda_1 = 0.55\ \mu$; +, measurements with searchlight probing.

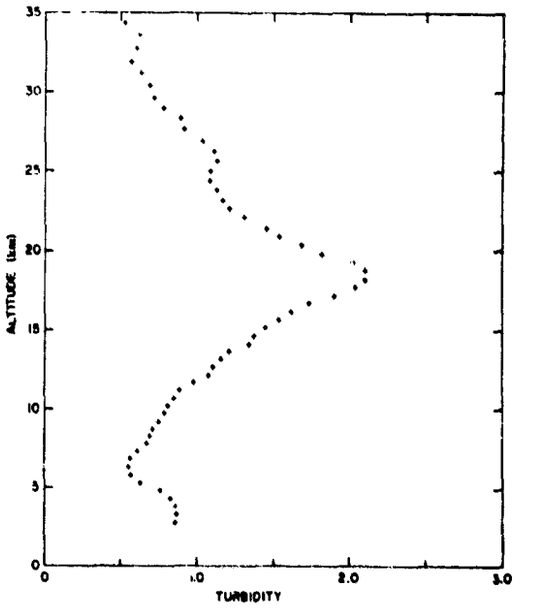

Fig. 5. Mean turbidity profile, $\bar{\beta}_p(h,\lambda_1)/\beta_r(h,\lambda_1)$ (see caption for Fig. 4).

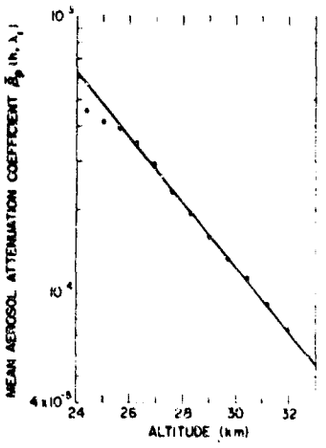

Fig. 6. The 26–32-km altitude region showing scale height H_p = 3.75 km for seventy-nine-profile mean; least square fit used to extrapolate to 50 km.

sea level. To establish upper altitude aerosol coefficients, a least-square fit was computed for $\bar{\beta}_p(h, \lambda_1)$ from 26 km to 32 km (Fig. 6). The result, H_p = 3.75 km (in effect derived from 790 measurement points), was used in Eq. (3) to extend the values to 50 km. Miller (1967) obtained H_p = 3.25 km from an analysis of rocket measurements acquired in 1964 for this altitude region. The over-all aerosol attenuation profile from sea level to 50 km is presented in Fig. 7. Rayleigh attenuation is included for comparison.

III. Atmospheric Attenuation

Previously, an atmospheric attenuation model was formulated (Elterman, 1964) for the uv, visible, and ir. It was based on Rayleigh (molecular) cross sections with number densities from the standard atmosphere (U.S. Standard Atmosphere, 1962) on ozone absorption coefficients (Vigroux, 1953) applied to a representative atmospheric ozone distribution; and on aerosol attenuation coefficients. The last were acquired from available but dissimilar measurements with interpolation used to establish a continuous aerosol profile. Since the aerosol parameters play an important role in computing atmospheric attenuation, the results here presented can be used for this application.

In Fig. 7, we developed the aerosol profile for altitudes to 50 km. It would be in order now to examine some expressions leading to corresponding aerosol profiles for attenuation at other wavelengths. If we consider a real atmosphere, the aerosol sizes within unit volume can be described by a size distribution function $\psi(r)$. Various size distribution functions are in use: the Junge type power law (1963) with a choice of exponents discussed in detail by Bullrich (1964), a similar distribution modified by gaps observed by Fenn (1964), a log-gaussian distribution used by Foitsik (1965), a composite distribution with components from several types. The optical-particle size relationship utilizes $\psi(r)$ such that

$$\beta_p(m,r,\lambda) = \int_{N_{r_2}}^{N_{r_1}} \sigma_p(m,r,\lambda)\,dN_p(r), \tag{4}$$

$$dN_p = N_0\psi(r)dr, \tag{5}$$

$$N_0(h) = CN_p(h); \tag{6}$$

β_p is the aerosol attenuation coefficient, m is the index of refraction, N_{r_1} and N_{r_2} are the aerosol number density limits established by the radii limits r_1 and r_2, σ_p is the aerosol cross section for each particle, N_p is the total number of particles between r_1 and r_2. For a given altitude, N_0 is actually proportional to the particle number density between r_1 and r_2. If the same size distribution function applies to all altitudes (a usual assumption), Eqs. (4), (5), and (6) are combined

$$\beta_p(h,\lambda) = CN_p(h)\int_{r_1}^{r_2} \sigma_p(r,\lambda)\psi(r)dr. \tag{7}$$

Here, $CN_p(h)$ is placed outside the integral which now contains only factors that are independent of altitude; also, m is removed because subsequent considerations will pertain to particles without any distinction in refractive index. If Eq. (7) is normalized to sea level conditions, the integral cancels out. Then, generally, for the various wavelengths λ, and specifically for λ_1 = 0.55 μ, we have

$$\frac{\beta_p(h,\lambda)}{\beta_p(0,\lambda)} = \frac{\beta_p(h,\lambda_1)}{\beta_p(0,\lambda_1)} = \frac{N_p(h)}{N_p(0)}, \tag{8}$$

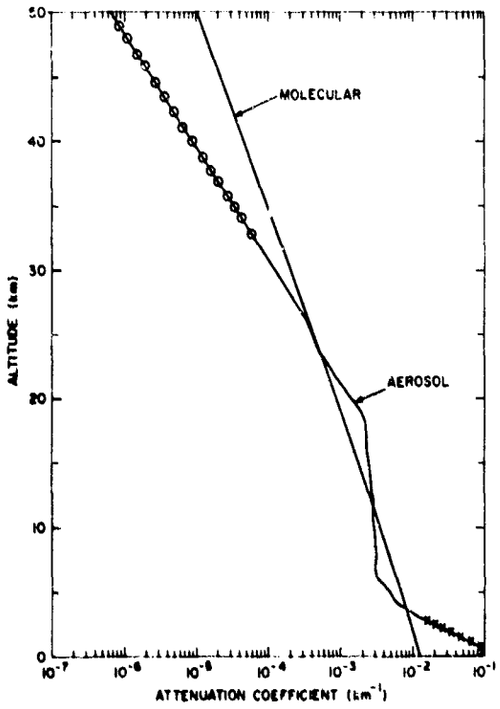

Fig. 7. Comparison of profiles. Mean aerosol attenuation coefficients $\bar{\beta}_p(h,\lambda_1)$ from measurements; molecular $\beta_r(h,\lambda_1)$ computed; λ_1 = 0.55 μ. ×, extrapolated 3.7 km to surface with H_p = 1.2 km; O, extrapolated 32–50 km with scale height H_p = 3.75 km.

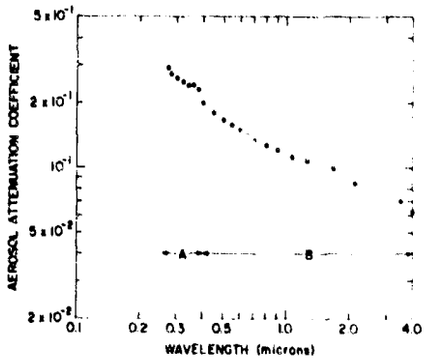

Fig. 8. Aerosol attenuation coefficients $\beta_p(0,\lambda)$ vs wavelength at sea level for a meteorological range approximating 25 km. *A*—derived from Baum and Dunkelman (1955); *B*—contained in Curcio *et al.* (1961).

$$\beta_p(h,\lambda) = \frac{\beta_p(0,\lambda)}{\beta_p(0,\lambda_1)}\,\beta_p(h,\lambda_1). \tag{9}$$

Equation (9) has been derived in this manner to demonstrate its compatibility with particle size considerations. Sea level conditions have been researched extensively by Curcio and Durbin (1959), Curcio *et al.* (1961), Knestrick *et al.* (1961), Dunkelman (1952), and Baum and Dunkelman (1955). The $\beta_p(0,\lambda)$ values for a 25-km meteorological range based on the results of these authors are shown in Fig. 8. Utilizing these results, in conjunction with the $\beta_p(h,\lambda_1)$ profile in Fig. 7, all requirements for the right-hand side of Eq. (9) are satisfied, and a series of aerosol attenuation profiles can be computed for 0–50-km altitudes and various wavelengths of interest. Since the pure air and ozone coefficients are available from the earlier publication (Elterman, 1964), revised tables of attenuation can be computed using Eq. (9) and

$$\tau_r(h,\lambda) = \sum_0^h \bar{\beta}_r(h,\lambda)\Delta h, \tag{10}$$

$$\tau_p(h,\lambda) = \sum_0^h \bar{\beta}_p(h,\lambda)\Delta h, \tag{11}$$

$$\tau_3(h,\lambda) = \sum_0^h \bar{\beta}_3(h,\lambda)\Delta h, \tag{12}$$

where τ_r, τ_p, and τ_3 are the Rayleigh, aerosol, and ozone optical thickness, respectively, from sea level to altitude h, and $\bar{\beta}_r$, $\bar{\beta}_p$, and $\bar{\beta}_3$ are the mean Rayleigh, aerosol, and ozone attenuation coefficients (km^{-1}), respectively, for the altitude interval Δh. Thus, a format can be used wherein the attenuation coefficients and computed optical thickness values due to pure air, ozone, and aerosols are tabulated individually. This format is advantageous because it permits various exploratory calculations (horizontal, vertical, and slant path) for each attenuating component or for over-all atmospheric extinction (pure air + ozone + aerosol).

Table II is an example of the format for the uv at 0.30 μ based on Eqs. (10), (11), and (12). The wavelength is characterized by severe O_3 absorption (Hartley band) so that for unit air mass, the optical thickness attributable only to O_3 is $\tau_3' = 3.4$ corresponding to a transmission of 3.3%.

Rayleigh scattering, because of the short wavelength, also contributes significantly to attenuation. For unit air mass, the Rayleigh optical thickness is 1.22 corresponding to 29.6% transmission. Also, for these conditions, the aerosol optical thickness is 0.41 corresponding to 67% transmission. Since all attenuating components are important, this tabulation demonstrates the interplay of attenuation coefficients as they vary with altitude.

Table III contains the parameters for 0.55 μ, the wavelength representing the photopic region. Absorption by O_3 (Chappuis band) now is diminished. However, the coefficients show that for some altitude regions, O_3 absorption can be larger than attenuation due to scattering by pure air or by aerosols. Comparing with Table II, for unit air mass, the optical thickness attributable only to O_3 is $\tau_3' = 0.03$ corresponding to a transmission approximating 97%. The Rayleigh optical thickness is 0.098 corresponding to about 91% transmission and the aerosol optical thickness is 0.25 corresponding to 88% transmission. The β_p column of this tabulation contains the digitized values of the aerosol profile in Fig. 7.

Attenuation parameters derived for twenty-two wavelengths in the uv, visible, and ir (from $\lambda = 0.27$ to 4.0 μ) for altitudes to 50 km are published elsewhere (Elterman, 1968).

IV. Interpretation of Profiles in the Troposphere

As mentioned, the aerosol attenuation profiles were obtained by measuring continuously through the troposphere and stratosphere. At the lower altitudes (starting with 2.8 km), the spread of the standard deviation limits is significantly larger than at 20 km (Fig. 4). It follows then that aerosol conditions in the troposphere are highly variable, compared with those in the stratosphere.

In spite of the variability, certain aerosol features in the troposphere can be discerned. As with the single profile (Figs. 2 and 3), the averages (Figs. 4 and 5) show the presence of a surface convective layer which extends to about 5 km during nights when measurements were taken. Using Stokes law for a particle diameter of 2 μ and the usual density approximation of 2 g/cm^3, the resulting fall speed is 2.6×10^{-2} cm/sec. Since aerosol diameters in the atmosphere generally are less than 2 μ, their descent during the night over a 12-h period is about 22 m or less. Hence, particles convected upward during the day should persist through the night.

The amount of dust is dependent on the cumulative effects of surface heating, so that the aerosol content in the surface convective layer should be seasonally dependent. Figure 9 demonstrates this seasonal dependency. During the spring and early summer, when the surface temperature exceeds the air temperature, the aerosol content in this layer is relatively high. During the winter months, the surface air temperature

Table II. Parameters at 0.30 μ

Alt. (km) h	Rayleigh atten. coeff. (km^{-1}) β_r	Rayleigh optical thick. (0 - h) τ_r	Rayleigh optical thick. (h - ∞) τ_r'	Aerosol atten. coeff. (km^{-1}) β_p	Aerosol optical thick. (0 - h) τ_p	Aerosol optical thick. (h - ∞) τ_p'	Ozone abs. coeff. (km^{-1}) β_3	Ozone optical thick. (0 - h) τ_3	Ozone optical thick. (h - ∞) τ_3'	Ext. coeff. (km^{-1}) β_{ext}	Ext. optical thick. ((0 - h) τ_{ext}	Ext. optical thick. (h - ∞) τ_{ext}'
0	1.446 -1	.000	1.222	2.00 -1	.000	.411	3.00 -2	.000	3.413	4.41 -1	.000	5.047
1	1.312 -1	.138	1.084	1.14 -1	.187	.224	2.27 -2	.034	3.379	2.79 -1	.360	4.660
2	1.189 -1	.263	.959	6.34 -2	.289	.142	2.05 -2	.066	3.347	1.96 -1	.598	4.450
3	1.078 -1	.376	.849	2.07 -2	.369	.107	2.52 -2	.093	3.320	1.53 -1	.773	4.274
4	9.772 -2	.477	.744	1.10 -2	.420	.091	2.23 -2	.117	3.295	1.31 -1	.915	4.132
5	8.693 -2	.569	.652	8.26 -3	.450	.081	2.23 -2	.140	3.273	1.18 -1	1.039	4.008
6	7.792 -2	.651	.570	5.83 -3	.337	.074	2.18 -2	.162	3.231	1.06 -1	1.151	3.897
7	6.955 -2	.725	.496	5.41 -3	.342	.069	2.23 -2	.184	3.229	9.76 -2	1.252	3.795
8	6.207 -2	.791	.431	5.38 -3	.348	.063	2.30 -2	.207	3.208	9.07 -2	1.346	3.701
9	5.513 -2	.849	.372	5.35 -3	.353	.058	2.84 -2	.232	3.180	8.89 -2	1.436	3.611
10	4.881 -2	.901	.320	5.22 -3	.358	.053	3.53 -2	.264	3.143	8.94 -2	1.525	3.522
11	4.306 -2	.947	.274	4.89 -3	.364	.047	4.05 -2	.305	3.107	9.44 -2	1.617	3.430
12	3.682 -2	.987	.235	5.13 -3	.369	.042	6.27 -2	.360	3.053	1.05 -1	1.717	3.331
13	3.147 -2	1.021	.201	4.74 -3	.373	.038	8.33 -2	.434	2.979	1.22 -1	1.830	3.218
14	2.690 -2	1.050	.171	4.54 -3	.378	.033	9.07 -2	.525	2.888	1.28 -1	1.955	3.093
15	2.299 -2	1.075	.147	4.35 -3	.383	.028	1.00 -1	.623	2.789	1.28 -1	2.083	2.965
16	1.965 -2	1.096	.125	4.15 -3	.387	.024	1.04 -1	.726	2.687	1.28 -1	2.210	2.837
17	1.680 -2	1.114	.107	4.10 -3	.391	.020	1.12 -1	.834	2.579	1.33 -1	2.341	2.707
18	1.436 -2	1.130	.092	3.97 -3	.395	.016	1.23 -1	.951	2.461	1.42 -1	2.478	2.569
19	1.223 -2	1.143	.078	3.34 -3	.399	.012	1.43 -1	1.085	2.326	1.59 -1	2.628	2.419
20	1.050 -2	1.154	.067	2.45 -3	.402	.009	1.56 -1	1.239	2.173	1.79 -1	2.797	2.250
21	8.937 -3	1.164	.057	1.78 -3	.404	.007	1.85 -1	1.415	1.993	1.97 -1	2.985	2.063
22	7.615 -3	1.172	.049	1.34 -3	.405	.006	1.99 -1	1.607	1.805	2.08 -1	3.187	1.860
23	6.433 -3	1.179	.042	1.02 -3	.406	.005	2.00 -1	1.807	1.606	2.07 -1	3.395	1.653
24	5.541 -3	1.185	.036	8.11 -4	.407	.004	1.95 -1	2.004	1.408	2.01 -1	3.599	1.448
25	4.732 -3	1.191	.031	6.83 -4	.408	.003	1.82 -1	2.193	1.220	1.87 -1	3.793	1.254
26	4.044 -3	1.195	.027	5.96 -4	.409	.002	1.65 -1	2.356	1.047	1.69 -1	3.972	1.076
27	3.458 -3	1.199	.023	4.55 -4	.409	.002	1.42 -1	2.519	.893	1.45 -1	4.129	.918
28	2.960 -3	1.202	.020	3.49 -4	.410	.001	1.24 -1	2.553	.760	1.28 -1	4.266	.781
29	2.535 -3	1.205	.017	2.68 -4	.410	.001	1.08 -1	2.769	.644	1.11 -1	4.386	.662
30	2.173 -3	1.207	.015	2.06 -4	.410	.001	9.12 -2	2.856	.544	9.36 -2	4.488	.560
31	1.864 -3	1.209	.013	1.57 -4	.410	.001	8.01 -2	2.954	.459	8.21 -2	4.576	.472
32	1.600 -3	1.211	.011	1.20 -4	.411	.000	6.89 -2	3.029	.394	7.06 -2	4.652	.395
33	1.386 -3	1.212	.009	9.22 -5	.411	.000	5.88 -2	3.092	.320	6.02 -2	4.717	.330
34	1.167 -3	1.213	.008	7.06 -5	.411	.000	4.90 -2	3.146	.266	5.02 -2	4.773	.275
35	9.990 -4	1.214	.007	5.41 -5	.411	.000	4.35 -2	3.193	.220	4.46 -2	4.820	.227
36	8.567 -4	1.215	.006	4.15 -5	.411	.000	3.83 -2	3.233	.180	3.74 -2	4.861	.186
37	7.360 -4	1.216	.005	3.18 -5	.411	.000	3.05 -2	3.266	.147	3.13 -2	4.895	.152
38	6.335 -4	1.217	.005	2.44 -5	.411	.000	2.50 -2	3.294	.119	2.62 -2	4.924	.123
39	5.461 -4	1.217	.004	1.86 -5	.411	.000	2.13 -2	3.318	.095	2.25 -2	4.948	.099
40	4.717 -4	1.219	.004	1.43 -5	.411	.000	1.89 -2	3.338	.075	1.93 -2	4.969	.078
41	4.080 -4	1.219	.003	1.09 -5	.411	.000	1.54 -2	3.355	.057	1.58 -2	4.987	.061
42	3.535 -4	1.219	.003	8.30 -6	.411	.000	1.20 -2	3.369	.046	1.24 -2	5.001	.046
43	3.068 -4	1.219	.002	6.40 -6	.411	.000	9.39 -3	3.380	.033	9.71 -3	5.012	.035
44	2.666 -4	1.219	.002	4.90 -6	.411	.000	7.51 -3	3.388	.025	7.79 -3	5.021	.027
45	2.321 -4	1.220	.002	3.75 -6	.411	.000	5.82 -3	3.395	.018	6.05 -3	5.028	.020
46	2.023 -4	1.220	.002	2.86 -6	.411	.000	4.50 -3	3.400	.013	4.71 -3	5.033	.014
47	1.767 -4	1.220	.001	2.21 -6	.411	.000	3.57 -3	3.404	.009	3.74 -3	5.037	.010
48	1.554 -4	1.220	.001	1.69 -6	.411	.000	2.82 -3	3.407	.006	2.98 -3	5.041	.007
49	1.373 -4	1.220	.001	1.29 -6	.411	.000	2.25 -3	3.410	.003	2.39 -3	5.043	.004
50	1.212 -4	1.221	.001	9.91 -7	.411	.000	1.88 -3	3.412	.001	2.00 -3	5.045	.002

Table III. Parameters at 0.55 μ

Alt. (km) h	Rayleigh atten. coeff. (km^{-1}) β_r	Rayleigh optical thick. (0 - h) τ_r	Rayleigh optical thick. (h - ∞) τ'_r	Aerosol atten. coeff. (km^{-1}) β_p	Aerosol optical thick. (0 - h) τ_p	Aerosol optical thick. (h - ∞) τ'_p	Ozone absorp. coeff. (km^{-1}) β_3	Ozone optical thick. (0 - h) τ_3	Ozone optical thick. (h - ∞) τ'_3	Ext. coeff. (km^{-1}) β_{ext}	Ext. optical thick. (0 - h) τ_{ext}	Ext. optical thick. (h - ∞) τ'_{ext}
0	1.162 -2	.000	.098	1.58 -1	.000	.250	3.23 -4	.000	.031	1.73 -1	.000	.379
1	1.055 -2	.011	.087	6.95 -2	.114	.136	3.00 -4	.000	.031	8.03 -2	.125	.154
2	9.550 -3	.021	.077	3.30 -2	.163	.086	2.70 -4	.001	.030	3.93 -2	.185	.124
3	8.627 -3	.030	.068	1.26 -2	.185	.065	2.30 -4	.001	.029	2.15 -2	.216	.103
4	7.774 -3	.038	.060	6.35 -3	.196	.055	2.08 -4	.001	.028	1.45 -2	.234	.095
5	6.987 -3	.045	.052	3.02 -3	.200	.049	2.03 -4	.001	.028	1.02 -2	.247	.092
6	6.263 -3	.052	.045	1.54 -3	.205	.045	1.99 -4	.001	.030	1.00 -2	.258	.121
7	5.598 -3	.058	.040	3.29 -3	.208	.042	2.05 -4	.002	.029	9.09 -3	.268	.111
8	4.989 -3	.064	.035	3.39 -3	.211	.038	2.10 -4	.002	.029	8.59 -3	.277	.102
9	4.431 -3	.069	.030	3.25 -3	.215	.035	2.59 -4	.002	.029	7.99 -3	.285	.094
10	3.923 -3	.072	.025	3.17 -3	.218	.032	3.22 -4	.002	.029	7.42 -3	.293	.086
11	3.461 -3	.076	.022	2.97 -3	.221	.029	4.23 -4	.003	.029	6.85 -3	.300	.079
12	2.960 -3	.079	.019	3.12 -3	.224	.026	5.71 -4	.003	.029	6.65 -3	.307	.073
13	2.529 -3	.082	.016	2.89 -3	.227	.023	7.77 -4	.004	.027	6.19 -3	.313	.066
14	2.152 -3	.084	.014	2.82 -3	.230	.020	8.80 -4	.005	.026	5.86 -3	.319	.060
15	1.848 -3	.086	.012	2.65 -3	.233	.017	9.14 -4	.006	.025	5.41 -3	.325	.054
16	1.579 -3	.088	.010	2.52 -3	.235	.015	9.48 -4	.007	.024	5.05 -3	.330	.049
17	1.350 -3	.090	.008	2.49 -3	.238	.012	1.02 -3	.008	.023	4.86 -3	.335	.044
18	1.154 -3	.091	.007	2.41 -3	.240	.010	1.12 -3	.009	.022	4.69 -3	.340	.040
19	9.867 -4	.092	.006	2.33 -3	.242	.007	1.31 -3	.010	.021	4.32 -3	.344	.035
20	8.435 -4	.093	.005	1.49 -3	.244	.006	1.54 -3	.011	.020	3.84 -3	.348	.031
21	7.183 -4	.094	.005	1.08 -3	.245	.004	1.69 -3	.013	.018	3.49 -3	.352	.027
22	6.121 -4	.094	.004	8.13 -4	.246	.003	1.81 -3	.015	.016	3.24 -3	.355	.024
23	5.219 -4	.095	.003	6.22 -4	.247	.003	1.82 -3	.016	.015	2.97 -3	.358	.021
24	4.453 -4	.095	.003	4.93 -4	.248	.002	1.78 -3	.016	.013	2.71 -3	.361	.018
25	3.803 -4	.096	.002	4.15 -4	.248	.002	1.66 -3	.020	.011	2.45 -3	.364	.015
26	3.230 -4	.096	.002	3.62 -4	.248	.001	1.50 -3	.022	.010	2.19 -3	.366	.013
27	2.780 -4	.096	.002	2.77 -4	.249	.001	1.30 -3	.023	.008	1.85 -3	.368	.011
28	2.379 -4	.097	.002	2.12 -4	.249	.001	1.13 -3	.024	.007	1.58 -3	.370	.009
29	2.038 -4	.097	.001	1.63 -4	.249	.001	9.84 -4	.025	.006	1.35 -3	.371	.008
30	1.747 -4	.097	.001	1.25 -4	.249	.000	8.31 -4	.026	.005	1.13 -3	.373	.007
31	1.493 -4	.097	.001	9.55 -5	.249	.000	7.30 -4	.027	.004	9.75 -4	.374	.006
32	1.285 -4	.097	.001	7.31 -5	.249	.000	6.27 -4	.026	.003	8.29 -4	.375	.005
33	1.098 -4	.097	.001	5.60 -5	.250	.000	5.35 -4	.028	.003	7.01 -4	.375	.004
34	9.391 -5	.098	.001	4.29 -5	.250	.000	4.46 -4	.029	.002	5.83 -4	.376	.003
35	8.030 -5	.098	.001	3.29 -5	.250	.000	3.97 -4	.029	.002	5.10 -4	.377	.003
36	6.886 -5	.098	.000	2.52 -5	.250	.000	3.32 -4	.029	.002	4.26 -4	.377	.002
37	5.916 -5	.098	.000	1.93 -5	.250	.000	2.76 -4	.030	.001	3.56 -4	.377	.002
38	5.092 -5	.098	.000	1.48 -5	.250	.000	2.33 -4	.030	.001	2.98 -4	.378	.002
39	4.390 -5	.098	.000	1.13 -5	.250	.000	2.00 -4	.030	.001	2.55 -4	.378	.001
40	3.791 -5	.098	.000	8.60 -6	.250	.000	1.71 -4	.030	.001	2.18 -4	.378	.001
41	3.279 -5	.098	.000	6.64 -6	.250	.000	1.40 -4	.031	.001	1.79 -4	.378	.001
42	2.841 -5	.098	.000	5.08 -6	.250	.000	1.09 -4	.031	.000	1.43 -4	.379	.001
43	2.466 -5	.098	.000	3.89 -6	.250	.000	8.56 -5	.031	.000	1.14 -4	.379	.001
44	2.143 -5	.098	.000	2.98 -6	.250	.000	6.84 -5	.031	.000	9.29 -5	.379	.000
45	1.866 -5	.098	.000	2.28 -6	.250	.000	5.30 -5	.031	.000	7.39 -5	.379	.000
46	1.626 -5	.098	.000	1.75 -6	.250	.000	4.10 -5	.031	.000	5.90 -5	.379	.000
47	1.420 -5	.098	.000	1.34 -6	.250	.000	3.25 -5	.031	.000	4.80 -5	.379	.000
48	1.249 -5	.098	.000	1.03 -6	.250	.000	2.57 -5	.031	.000	3.92 -5	.379	.000
49	1.103 -5	.098	.000	7.86 -7	.250	.000	2.05 -5	.031	.000	3.23 -5	.379	.000
50	9.743 -6	.098	.000	6.02 -7	.250	.000	1.71 -5	.031	.000	2.75 -5	.379	.000

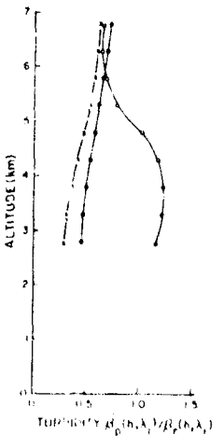

Fig. 9. Monthly averages for surface convective layer. Turbidities computed from measurements; $\lambda_1 = 0.55\,\mu$; ×, five profiles, December 1964; ●, twenty-three profiles, December 1963; ○, twenty-nine profiles, April 1964.

differential is reversed, and this tends to suppress the vertical transport of aerosols from the surface.

Above the surface convective layer, aerosols are transported vertically toward the tropopause due to mixing and convection. At such times when the aerosols reach a stable layer or the tropopause, their further vertical transport is inhibited. Usually, convection and mixing tend to establish a constant turbidity. However, aerosol depletion by the washout effects of precipitation is greater in the lower troposphere than in the upper. Accordingly, a turbidity maximum occurs frequently below the tropopause.

V. Interpretation of Profiles in the Stratosphere

In order to develop this topic, we note first that the character of the tropopause relates to the history of its air mass. In tropical regions the tropopause is located near 18 km and is characterized by a temperature minimum in the vicinity of −80°C. Over temperate latitudes, the tropopause is frequently found near 12 km with temperatures near −50°C. Owing to advection, a temperature minimum near 18 km often is discernible in temperature latitudes. In this paper, we refer to the lower tropopause as the polar tropopause and it is identified as the base of a stable region. The temperature minimum at the higher altitude will be designated as the tropical tropopause. The region between them is considered as part of the stratosphere.

In Fig. 10, two features are demonstrated from nightly mean profiles and their concurrent temperature soundings. It is seen that a maximum in turbidity is located near the tropical tropopause and a secondary maximum below the polar tropopause. These features occurred almost invariably in all the profiles whenever both polar and tropical tropopauses were in evidence. The altitude relationship between the turbidity maximum and the tropical tropopause is shown in Fig. 11. Here the monthly average altitudes of the turbidity maxima are compared with the average altitudes of the tropical tropopause (from concurrent soundings) for eleven months during the period December 1963 to April 1965 when data were available. The comparison shows the relationship to be almost linear. For the entire period, the altitude of the turbidity maximum averages 1.4 km below that of the temperature minimum.

In Fig. 12, the presence of a seasonal trend is examined. The stratospheric turbidity is relatively high during the period December 1963 to February 1964, becomes a minimum in April, and actually rises to a maximum for the period in June 1964. From October to April 1965, there is a descending trend. The trend of the temperature minima is similar to the turbidities for the entire period. As discussed in Sec. II, the high turbidity values during the early part of the period may

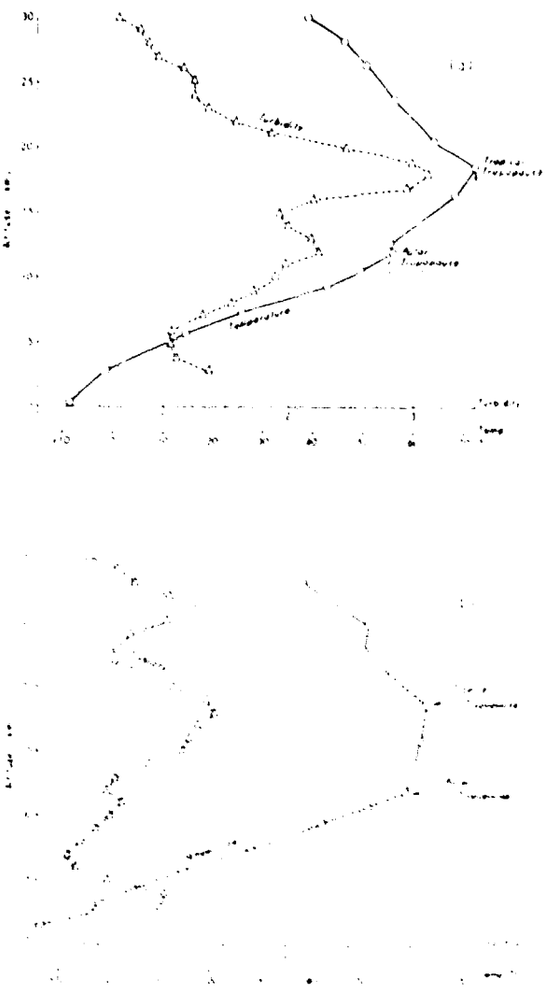

Fig. 10. Mean turbidity profiles with concurrent temperature soundings showing turbidity-temperature relationships. (a) Average of five turbidity profiles for 8–9 April, 1964; (b) average of six turbidity profiles for 12–13 April 1964.

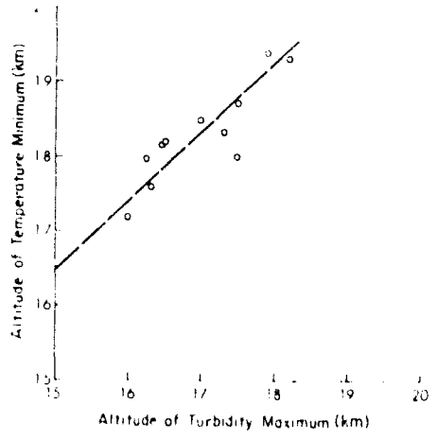

Fig. 11. Relationship between altitude of stratospheric turbidity maximum and altitude of tropical tropopause (temperature minimum). Each circle is a monthly average.

be due partially to the presence of volcanic dust from the March 1963 eruption.

Figure 12 demonstrates the presence of another significant feature; i.e., a temperature turbidity relationship. As the minimum temperature of the tropopause changes, the magnitude of the turbidity also changes in an inverse way. When temperature minima are low (December 1963, June and October 1964) turbidity values are high, whereas with warmer temperature minima, the turbidities are lower. A further indication of the turbidity–temperature relationship is seen in Fig. 10(a), where the temperature minimum is $-71°C$ at 18.5 km and the turbidity maximum $\beta_r\ \beta_r = 3.0$; in Fig. 10(b), four days later, a different air mass is evident, with a temperature minimum $-62°C$ at 19 km. The corresponding turbidity $\beta_r\ \beta_r = 1.5$. Thus the stratospheric aerosol content can change sharply in a few days with changes in temperature which are caused by changes in the general circulation.

In summary, the optical probing measurements over New Mexico show that the following relationships occur.

(1) a turbidity maximum is located below the polar tropopause;

(2) a turbidity maximum in the 16–19-km altitude region is located an average 1.4 km below the tropical tropopause;

(3) as the temperature of the tropical tropopause decreases, the magnitude of the turbidity maximum increases.

These relationships indicate that the turbidity is greatest in air originating from the tropics. The findings are consistent with those of Rosen (1968), whose results show the stratospheric aerosol concentrations are higher in tropical latitudes (Panama) than in temperate (Minneapolis). Our findings indicate, further, that the aerosols from or near the surface are convected through the troposphere in the manner already described in Sec. IV. Convective activity is more intense over tropical and subtropical regions where aerosols are transported vertically to altitudes of the tropical tropopause. Here temperatures are in the vicinity of $-80°C$. The air containing the aerosols then undergoes advection to temperate latitudes which accounts for the stratospheric feature: high turbidity accompanied by low temperature, at these latitudes.

There appears to be no basis for distinguishing between the 20-km dust layer and the aerosol concentrations occurring at altitudes between 16–19 km observed with optical probing over New Mexico. Accordingly, the existence of the layer is explained as a balance between depletion by fallout, diffusion, and the continued replenishment due to convection advection on the scale of the general circulation. If the major constituent of this layer is the ammonia sulfate particle, then its origin remains conjectural. Industrial pollution is discounted because nearly all of it is located in temperate latitudes, whereas the results show that tropical air is the transport medium. Additionally, although much of the tropics is covered by ocean which contains about 10% sulfates in solution, this is an unlikely source, because there is no known selective process which adequately favors transport of sulfate over sodium chloride found to be 77% in solution. Of interest are the speculations of Meinel and Meinel (1967) that SO_2 produced from volcanoes undergoes a series of aerochemical reactions yielding an ammonia sulfate layer at 26 km. To be consistent with our findings, such volcanic activity should occur at tropical and subtropical latitudes. This directs our attention to the continuous emissions of H_2S and SO_2 from the many fissures and fumaroles that characterize the 6400-km Indonesian belt of volcanic activity, as well as the volcanism in and about Central America.

Another turbidity maximum at 26 km occurred with sufficient frequency to be identified easily in Fig. 5. This altitude, then, was the basis for choosing the 25-km limit in Eq. (2). The measurements show that the

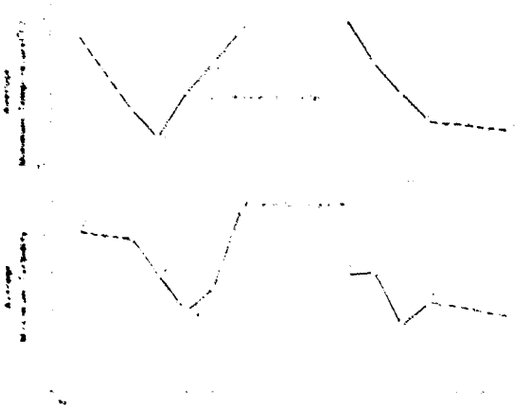

Fig. 12. Seasonal variations in the stratosphere, optical probing measurements compared with concurrent temperature soundings. The dashed lines indicate absence of data for intermediate months. Averages for July, August, and September are omitted due to insufficient data.

turbidity region extended from 25.0 km to 27.6 km and from April 1964 to December 1964 with the aerosol optical thickness averaging $\tau_p \simeq 10^{-3}$ for $\lambda_1 = 0.55\ \mu$. The existence of an aerosol concentration above 20 km is established by photography of the twilight aureole obtained by Gemini IV on 4 June 1965, subsequently analyzed by Mateer *et al.* (1967). However, owing to insufficient information, their analysis could not provide adequate altitude data. Examination of concurrent temperature profiles shows that generally the air is uniformly stable in this altitude region, so that no accumulation of aerosols should occur. The 26-km maximum was prominent during the eight-month period, April to December 1964, when Mt. Agung dust was diminished. This suggests that the phenomenon may be related to the process of volcanic dust abatement.

In the stratospheric region from 28 km to 70 km, a review of unreduced searchlight optical probing data does not reveal the presence of important aerosol concentrations.

VI. Concluding Remarks

A statistical treatment of data comprising 119 aerosol attenuation profiles provides information on aerosol attenuation coefficients, optical mixing ratios, stratospheric dust of volcanic origin and its abatement. These in turn permit examination of relative aerosol concentrations or layer features, aerosol scale height, and the determination of atmospheric attenuation parameters to 50 km.

The procedure for developing the aerosol attenuation parameters is summarized as follows.

(1) Various studies were compared and of these a set of aerosol measurements was selected.

(2) The choice of measurements (comprising 119 profiles from 2.76 km to 34.4 km) was examined statistically. This resulted in the elimination of forty profiles (December 1963 to March 1964 inclusive) characterized by a high volcanic dust component.

(3) The mean of the seventy-nine remaining profiles was extended to sea level and to 50 km, respectively, by reasonably supported extrapolations.

(4) The over-all profile then was developed laterally to obtain additional profiles for wavelengths of interest.

A significant aspect of the procedure is that the wavelength–height array of parameters was derived independently of the assumptions associated with conversion of a size distribution to an optical parameter.

Frequently, the attenuation profiles reflect short-term changes, especially at low altitudes; whereas stratospheric features appear less changeable. Individual and averaged aerosol attenuation profiles yield results which are compatible with known atmospheric processes. Because of the amount of data acquired, it has been possible to establish relationships between aerosol features and the atmospheric environment in which they exist.

The authors would like to express their appreciation to R. W. Fenn and R. Penndorf for their review and suggestions, to F. E. Volz for discussions pertaining to volcanic dust, and to R. Hoffman and J. Fusco for their participation with the computer programming.

Bibliography

W. A. Baum and L. Dunkelman, J. Opt. Soc. Amer. **45**, 166 (1955).
E. K. Bigg, Tellus, **16**, 77 (1964).
K. Bullrich, in *Advances in Geophysics*, H. E. Landsberg and J. E. Mieghem, Eds. (Academic Press Inc., New York, 1964), Vol. 10, pp. 101–257.
B. R. Clemesha, G. S. Kent, and R. W. Wright, J. Appl. Meteorol. **6**, 386 (1967).
R. T. H. Collis and M. G. H. Ligda, J. Atmos. Sci. **23**, 255 (1966).
P. Crosby and B. V. Koerber, J. Opt. Soc. Amer. **53**, 358 (1962).
J. A. Curcio and K. A. Durbin, "Atmospheric Transmission in the Visible Region," NRL Rept. 5362 (U.S. Naval Research Laboratory, Washington, D.C., 1959).
J. S. Curcio, G. L. Knestrick, and T. H. Cosden, "Atmospheric Scattering in the Visible and Infrared," NRL Rep. 5567 (U.S. Naval Research Laboratory, Washington, D.C., 1961).
A. Y. Driving, Izv. Atmos. Oceanic Phys., **2**, 1046–1054 (1966) (U.D.C. 551.593.5:629.195).
L. Dunkelman, "Horizontal Attenuation of Ultraviolet and Visible Light by the Lower Atmosphere," NRL Rep. No. 4031 (U.S. Naval Research Laboratory, Washington, D.C. 1952).
A. J. Dyer and B. B. Hicks, Nature **208**, 131 (1965).
L. Elterman, "Atmospheric Attenuation Model, 1964, in the Ultraviolet, Visible, and Infrared Regions for Altitudes to 50 km," Rep. AFCRL-64-740 (AFCRL, Bedford, Mass., 1964).
L. Elterman, Appl. Opt. **59**, 1769 (1966a).
L. Elterman, "An Atlas of Aerosol Attenuation and Extinction Profiles for the Troposphere and Stratosphere," Rep. AFCRL-66-828 (AFCRL, Bedford, Mass., 1966b).
L. Elterman, "UV, Visible and IR Attenuation to 50 km," Rep. AFCRL 68-0153 (AFCRL, Bedford, Mass., 1968).
R. W. Fenn, Beitr. Phys. Atmos. **34**, 69 (1964).
K. P. Feoktistov, G. P. Rozenberg, A. B. Sandomirskii, V. N. Sergevich, and D. M. Sonechkin, in *Issledovaniia komicheskogo prostranstva* (*Investigations of Cosmic Space*), G. A. Skuridin, Ed. (Ixd-vo Nauka Moscow, 1965), pp. 62–64.
L. Foitzik, Gerl. Beitr. Geophys. **73**, 199 (1965).
J. P. Friend, "Properties of the Stratospheric Aerosol," Isotopes, Inc. Report for contract DA-49-146-XZ-079 Defense Atomic Support Agency (U) (2 Nov. 1965).
G. Grams and G. Fiocco, J. Geophys. Res. **72**, 3523 (1967).
C. E. Junge, C. W. Chagnon, and J. E. Manson, J. Meteorol. **18**, 81 (1961).
C. E. Junge, *Air Chemistry and Radioactivity* (Academic Press Inc., New York, 1963).
G. L. Knestrick, T. H. Cosden, and J. A. Curcio, "Atmospheric Attenuation Coefficients in the Visible and Infrared," NRL Rep. 5648 (U.S. Naval Research Laboratory, Washington, D.C., 1961).
K. Ya. Kondratiev, G. A. Nicolsk, I. Ya. Badinov, and S. D Andrew, Appl. Opt. **6**, 197 (1967).
C. L. Mateer, J. V. Dave, L. Dunkelman, and D. C. Evans, "Evidence of an Upper Stratospheric Dust Layer in a Satellite Twilight Color Photograph," Rep. X-613-67-533 (Goddard Space Flight Center, Greenbelt, Md., 1967).
A. B. Meinel and M. P. Meinel, Nature **201**, 657 (1964).
A. B. Meinel and M. P. Meinel, Science **155**, 189 (1967).
D. E. Miller, Proc. Roy. Soc. London **A301**, 57 (1967).
S. C. Mossop, Nature **203**, 824 (1964).
G. Newkirk, Jr., and J. Eddy, J. Atmos. Sci. **21**, 35 (1964).

R. Penndorf, "The Vertical Distribution of Mie Particles in the Troposphere," Geophys. Res. Paper No. 25 (AFCRL, Bedford, Mass., 1954).
J. Rosen, J. Geophys. Res. **73**, 479 (1968).
G. V. Rozenberg, Ed. *Prozhektornyi luch v atmosfere* (*Searchlight Beams in the Atmosphere*), (Izd-vo AN SSSR, Moskow, 1960).
G. V. Rozenberg, *Twilight* (Plenum Press, Inc., New York, 1965).
G. V. Rozenberg, Paper presented at the International Conference on the Investigation of Noctilucent Clouds, Tallin, 1966.
A. B. Sandomirskii, N. P. Al'tovskaia, and G. I. Trifonova, Izv. AN SSSR, Ser. Geofiz. No. 7, 1121 (1964).
D. Spa...huch, Beitr. Phys. Atmos. **40**, 1, 2, 95, 117 (1967).
E. Vigroux, Ann. Phys. **8**, 709 (1953).
F. E. Volz and R. M. Goody, J. Atmos. Sci. **19**, 385 (1962).
F. E. Volz, Tellus **17**, 513 (1965).
J. M. Waldram, J. Meteorol. **71**, 319 (1945).
U.S. Standard Atmosphere 1962 (U.S. Govt. Printing Office, Washington D.C., 1962).

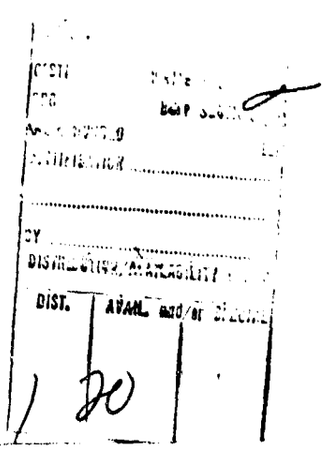

Unclassified
Security Classification

DOCUMENT CONTROL DATA - R&D

(Security classification of title, body of abstract and indexing annotation must be entered when the overall report is classified)

1. ORIGINATING ACTIVITY *(Corporate author)*
Air Force Cambridge Research Laboratories (CRO)
L.G. Hanscom Field
Bedford, Massachusetts 01730

2a. REPORT SECURITY CLASSIFICATION
Unclassified

2b. GROUP

3. REPORT TITLE

FEATURES OF TROPOSPHERIC AND STRATOSPHERIC DUST

4. DESCRIPTIVE NOTES *(Type of report and inclusive dates)*
Scientific, Interim.

5. AUTHOR(S) *(First name, middle initial, last name)*
L. Elterman
R. Wexler
D. T. Chang

6. REPORT DATE
January 1970

7a. TOTAL NO. OF PAGES
11

7b. NO. OF REFS
41

8a. CONTRACT OR GRANT NO.

b. PROJECT, TASK, WORK UNIT NOS. 7621-08-01

c. DOD ELEMENT 62101F

d. DOD SUBELEMENT 681000

9a. ORIGINATOR'S REPORT NUMBER(S)
AFCRL-70-0030

9b. OTHER REPORT NO(S) *(Any other numbers that may be assigned this report)*

10. DISTRIBUTION STATEMENT
1—This document has been approved for public release and sale; its distribution is unlimited.

11. SUPPLEMENTARY NOTES
Reprinted from Applied Optics. Vol. 8, pp. 893-903, No. 5, May 1969.

12. SPONSORING MILITARY ACTIVITY
Air Force Cambridge Research Laboratories (CRO)
L.G. Hanscom Field
Bedford, Massachusetts 01730

13. ABSTRACT

A series of 119 profiles obtained over New Mexico comprise aerosol attenuation coefficients vs altitude to about 35 km. These profiles show the existence of several feature. A surface convective dust layer extending up to about 5 km is seasonally dependent. Also, a turbidity maximum exists below the tropopause. The altitude of ar aerosol maximum in the lower stratosphere is located just below that of the minimum temperature. The colder the minimum temperature, the greater is the aerosol content of the layer. This relationship suggests that the 20-km dust layer is due to convection in tropical air and advection to higher latitudes. Computed averages of optical thickness show that abatement of stratospheric dust from the Mt. Agung eruption became evident in April 1964. Results based on seventy-nine profiles characterizing dust abatement indicate that above 26 km, the aerosol scale height averages 3.75 km. Extrapolating with this scale height, tabulations are developed for uv, visible, and ir attenuation to 50 km. Optical mixing ratios are used to examine the aerosol concentrations at various altitudes, including a layer at 26 km having an optical thickness 10^{-3} for 0.55-μ wavelength.

73

Unclassified
Security Classification